ADVANCED ENERGY MATERIALS
www.advenergymat.de

Hierarchically Self-Assembled MOF Network Enables Continuous Ion Transport and High Mechanical Strength

Lulu Du, Bo Zhang, Wei Deng, Yu Cheng, Lin Xu, and Liqiang Mai**

Composite solid electrolytes have attracted significant interest because they overcome the defects of single-component solid electrolytes. However, the discontinuous ion transport and weak mechanical support caused by randomly distributed powders lead to inferior ionic conductivity and poor mechanical strength. Herein, a hierarchically self-assembled metal-organic framework (MOF) network is designed to provide continuous ion transport and mechanical support for composite polymer electrolytes. This unique structure is achieved by constructing well-ordered MOF nanocrystals along 1D polyimide fibers to provide continuous linear pathways for lithium ions at the micrometer scale, and the 1D MOF fibers are interconnected to form a monolithic 3D network for continuous Li^+ transport in the bulk of composite electrolytes. Meanwhile, sub-nano pores and Lewis acid sites in MOF nanocrystals can selectively confine the movement of larger anions as ion sieves to promote Li^+ transport. In addition, the strong banding between MOF and polyimide, coupled with the robustness of the polyimide skeleton, endows the MOF network with high mechanical strength and flexibility. Accordingly, the resultant composite electrolyte delivers a high ionic conductivity and desired mechanical strength. This work shows that rational spatial arrangement of incorporated powders from disorder to order by a self-assembly strategy can yield novel properties for composite solid electrolytes and solid-state lithium batteries.

1. Introduction

The macroscopic properties of materials are not only associated with inherent characteristics of atoms/molecules, but also their spatial arrangement.[1,2] A structural unit showing a specific function can serve as a functional unit, ranging from atom/molecule system to microscale object.[3] Self-assembly refers to the fact that functional units spontaneously form well-ordered structures, which is ubiquitous in nature, like high-strength nacre, highly anisotropic and strong muscles, self-cleaning lotus effect.[4–7] The secret of these unique properties is the well-ordered structures formed by self-assembly process. Inspired by this, self-assembled artificial materials with revolutionary performances hold great promise in the field of energy storage and conversion.[8–10]

In this regard, the incorporated ionic conductors in composite polymer electrolytes can be considered as functional units, which have been used to improve electrochemical properties, structural stability, and mechanical robustness.[11–13] Conventionally, the most incorporated ionic conductors are ceramic particles, such as perovskite-type $Li_{0.33}La_{0.557}TiO_3$ (LLTO),[14] garnet-type $Li_7La_3Zr_2O_{12}$ (LLZO),[15] NASICON-type $Li_{1.3}Al_{0.3}Ti_{1.7}(PO_4)_3$ (LATP), $Li_{1.5}Al_{0.5}Ge_{1.5}(PO_4)_3$ (LAGP).[16] Recently, MOF impregnated with ionic liquid (IL) or liquid electrolyte has been served as a novel ionic conductor due to its internal massive pores, which can provide well-ordered ion pathways.[17–20] And some MOF materials are used as fillers for solid polymer electrolytes to enhance the ionic conductivity.[21] However, these discrete particles in polymer electrolytes usually lead to insufficient ionic conductivity improvement because of the isolated and discontinuous lithium ions channels.[22,23] Based on this, 1D ionic conductors with high aspect ratio have been designed and fabricated for extended ions pathways, such as nanowires,[24] nanofibers,[25] and nanotubes.[26] Unfortunately, the ionic conductivity enhancement is still limited, because the obtained composites are fabricated by incorporating above powders into polymer electrolytes, in which these incorporated powders are prone to aggregate and precipitate along with solvent volatilization in the film-forming process, leading to heavy barriers for continuous ion conduction.[27–29] In addition, the randomly distributed powders in polymer electrolytes fail to provide strong support for lithium dendrite suppression.

In order to overcome the issues of randomly distributed powders, some researchers pay attention to the spatial arrangement of incorporated ceramics in composite polymer

L. L. Du, W. Deng, Y. Cheng, L. Xu, L. Q. Mai
State Key Laboratory of Advanced Technology for Materials Synthesis and Processing
School of Materials Science and Engineering
Wuhan University of Technology
Luoshi Road 122, Wuhan 430070, P. R. China
E-mail: linxu@whut.edu.cn; mlq518@whut.edu.cn

B. Zhang
State Key Laboratory of Advanced Technology for Materials Synthesis and Processing
International School of Materials Science and Engineering
Wuhan University of Technology
Wuhan 430070, P. R. China

L. Xu, L. Q. Mai
Foshan Xianhu Laboratory of the Advanced Energy Science and Technology Guangdong Laboratory
Foshan 528200, P. R. China

The ORCID identification number(s) for the author(s) of this article can be found under https://doi.org/10.1002/aenm.202200501.

DOI: 10.1002/aenm.202200501

electrolytes by constructing 3D ceramic networks, in which the randomly distributed ceramic powders are designed to form 3D structures.[30–32] Despite the ions pathways can be significantly extended and agglomeration issue can be avoided, precise control of 3D networks with well-ordered structure, still remains a challenge in respect to the complicated reaction and harsh reaction condition. In addition, these 3D ceramic networks generally need high-temperature sintering process to ensure complete crystallization and removal of organic additives, which severely diminishes the mechanical strength.[33,34] As a result, the intrinsic brittleness of 3D ceramic networks makes them mechanically too fragile to maintain structure stability during polymer matrix permeation, battery assembly, and practical implementation. Therefore, it is of great importance to fabricate 3D ion conductors with well-ordered structure and high mechanical strength to achieve continuous ion transport and simultaneously strengthen the whole composites to effectively resist the dendrites growth.[35]

Here, we design a hierarchically self-assembled MOF network for polymer electrolytes, which aims to afford continuous ion transport and high mechanical strength. This hierarchically self-assembled MOF network is constructed by growing continuous MOF nanocrystals on 3D cross-linked network composed of 1D polyimide fibers, which offer the spatial guidance for self-assembly of MOF nanoparticles. In an effort to conduce to the oriented self-assembly of MOF nanocrystals, we develop a surface-etching strategy to form carboxylated polyimide, which can provide rich and homogeneous nucleation sites for well-ordered MOF growth. Zeolite imidazole framework (ZIF-8) is adopted as the targeted MOF because of its low cost, facile synthesis, and superior electrochemical stability. Besides, rich pores in ZIF-8 can immobilize ionic liquid in confined space, which realizes the transformation from inert conductors to ionic conductors. And the ionic liquid we selected is 1-ethyl-3-methylimidazolium bis(trifluoromethylsulfonyl)imide (EMIMTFSI), which is a highly conductive and nonflammable ionic liquid with low viscosity and wide electrochemical window. After encapsulating IL into the MOF network (MOF@IL), the micropores and Lewis acid sites inside the MOF network can optimize Li^+ transport. Subsequently, permeated with poly(vinylidene fluoride) (PVDF) polymer electrolyte, the resultant composite delivers an high ionic conductivity (4.08×10^{-4} S cm^{-1} at 30 °C), coupled with high mechanical strength. Furthermore, the assembled Li-Li cells perform well without short circuit and the $LiFePO_4$//Li cells maintain a remarkable capacity retention of 96.0% after 500 cycles at 0.5 C rate, merely decaying from 152.6 to 146.6 mAh g^{-1} at room temperature.

2. Results and Discussion

With the assistance of the self-assembly process, the ion-conducting 3D hierarchical network in macroscale can be obtained after impregnating with Li^+-containing IL (**Scheme 1**). This monolithic 3D ion conductor consists of interconnected 1D MOF fibers, forming a unique hierarchical structure. At the micrometer scale, each 1D MOF fiber is composed of well-ordered MOF nanocrystals along the 1D direction, which can provide continuous linear pathways for Li^+ to transfer for a long distance without obstacles. More importantly, sub-nano pores in MOF nanocrystals can spatially confine the movement of larger anions as ion sieves to promote Li^+ transport, and the open metal sites showing Lewis acid feature enable the selective bonding of $TFSI^-$, thus endowing fast Li^+ transport. And the preparation process of the composite solid electrolyte based on the hierarchically self-assembled MOF network is shown in **Figure 1**a. Polyimide fibrous nonwoven was elaborately selected as the pristine skeleton because of its ideal mechanical strength,

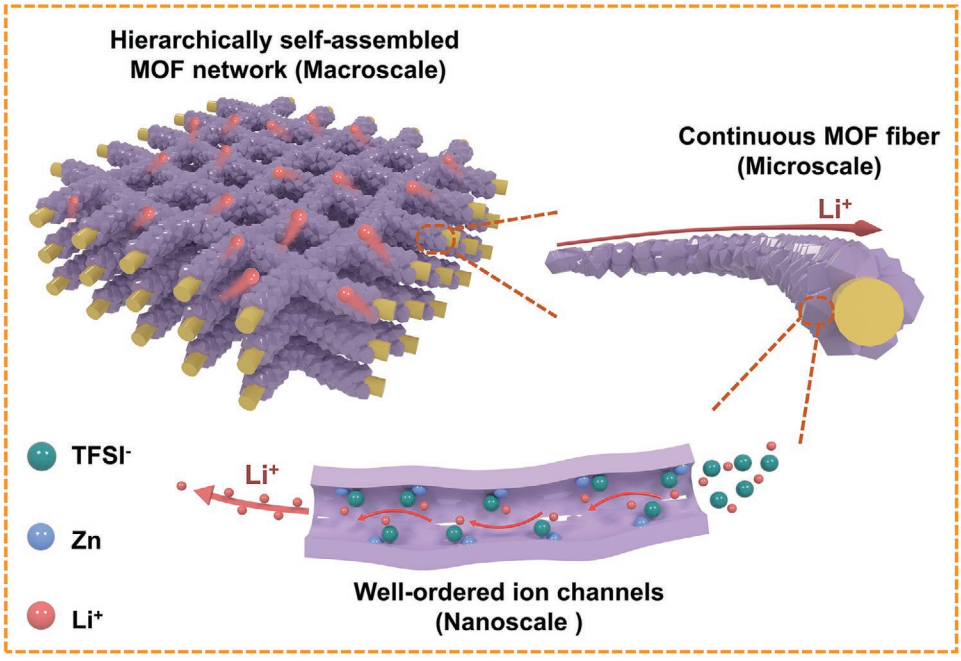

Scheme 1. Schematic illustration of hierarchically self-assembled MOF network as 3D ion conductor with continuous Li^+ transport.

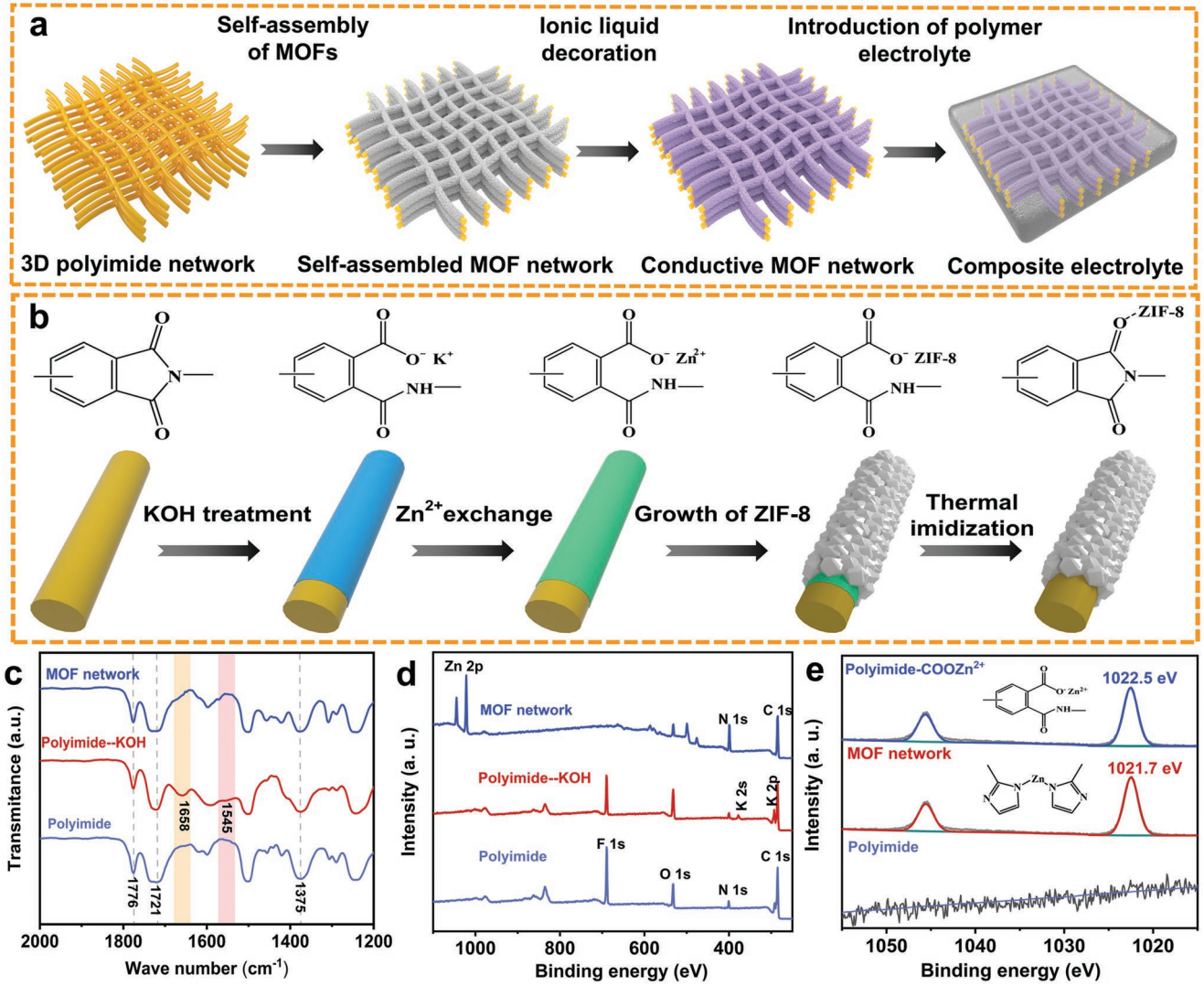

Figure 1. Design and synthesis of hierarchically self-assembled MOF network reinforced polymer electrolyte. a) Schematic diagram of preparation process of the composite solid electrolyte based on hierarchically self-assembled MOF network. b) Schematic of the self-assembly process. c) FTIR spectra of polyimide, polyimide after KOH treatment and MOF network after thermal treatment. d) XPS survey spectra of polyimide, polyimide after KOH treatment and MOF network after thermal treatment. e) High-resolution Zn 2p XPS spectra of polyimide, polyimide after Zn^{2+} exchange, and MOF network after thermal treatment.

electric insulation, thermal and electrochemical stability,[36–38] which was composed of 1D fibers with a cross-linked structure. And the large pores between interconnected fibers are beneficial to the full infiltration of PVDF-bis(trifluoromethane)sulfonimide lithium salt (LiTFSI) for a dense electrolyte. Then the MOF (ZIF-8) nanoparticles were self-assembled on the polyimide substrate via in situ growth method to form the hierarchically self-assembled MOF network. After encapsulating the Li-containing IL inside the pores of MOF, the original MOF network transformed into a 3D ion conductor. Finally, the resultant composite solid electrolyte can be obtained after infiltration of PVDF-LiTFSI polymer electrolyte into the Li^+-conducting MOF network (denoted as MOF network-PVDF).

Of note, self-assembly process is imperative to form the continuous ion conduction in the bulk of composite electrolytes. Based on this, a surface-etching method was developed to enable the oriented self-assembly of MOF nanocrystals (Figure 1b). Through etching in KOH solution, imide-ring cleavage reactions produce a large number of carboxyl groups on the surface of polyimide substrate,[39] which provide massive and uniform nucleation sites to form the well-ordered and continuous MOF network. After immersing in $Zn(NO_3)_2$ methanol solution, Zn^{2+} was ion-exchanged with K^+ followed by in situ growth of ZIF-8 nanoparticles via coordination of ligand 2-methylimidazole (2-MIN). Finally, thermal treatment was conducted to re-cyclize the cleaved imide rings on the surface of polyimide and simultaneously activate the self-assembled MOF network by removing the residual solvent. In order to better investigate the composition of the hierarchically self-assembled MOF network, the diffraction pattern of the hierarchically self-assembled MOF network was compared with the simulated ZIF-8, and was consistent with the simulated ZIF-8,

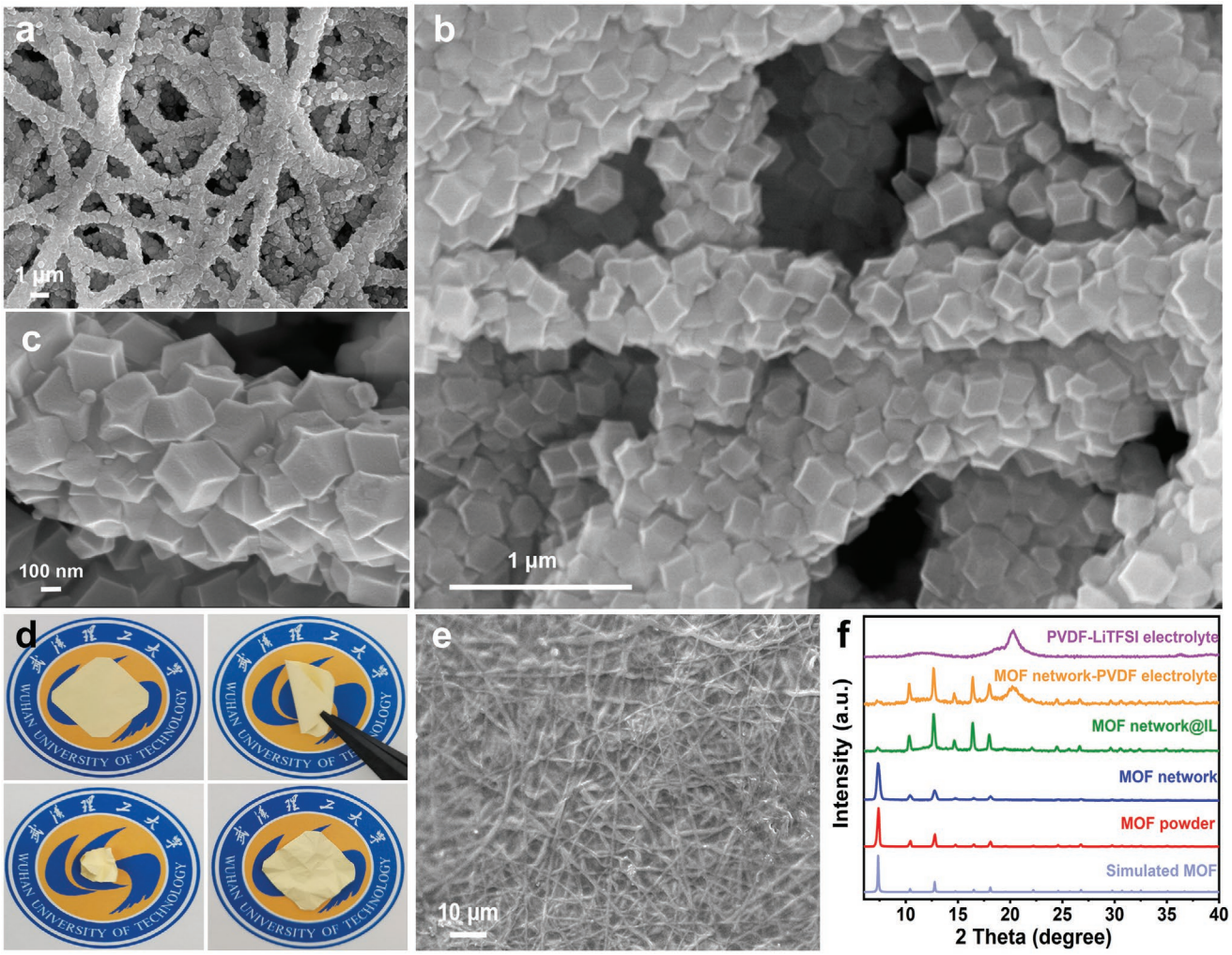

Figure 2. Structural characterizations of hierarchically self-assembled MOF network reinforced polymer electrolyte. a–c) SEM images of Hierarchically self-assembled MOF network. d) Photos of the hierarchically self-assembled MOF network being flat, bent, squeezed, and after. e) SEM image of MOF network-PVDF composite solid electrolyte. f) XRD patterns of MOF network-PVDF and related materials.

which indicated the successful fabrication of the MOF network with high-quality crystalline structure (**Figure 2**f).

In order to investigate the mechanism of the self-assembly process, Fourier transform infrared (FTIR) spectra technique was applied as shown in Figure 1c and Figure S1 (Supporting Information). Pristine polyimide shows characteristic bands at 1776 and 1721 cm^{-1} (C=O antisymmetric and symmetric swing vibrations), coupled with 1375 cm^{-1} (C—N—C stretching vibrations of imide rings). After KOH treatment, new peaks at 1647 cm^{-1} (C=O stretching) and 1539 cm^{-1} (N—H mixed mode) indicate imide rings are cleaved in —COOK and —NH.[40,41] In addition, the sharp peak at 1375 cm^{-1} becomes broader because of the newly formed —COOK. After thermal treatment, the curve of the self-assembled MOF network is akin to that of the pristine polyimide, indicating the effectiveness of the surface-etching self-assembly method. Besides, X-ray photoelectron spectroscopy (XPS) was also carried out to confirm above discussions. As shown Figure 1d, merely C 1s, N 1s, O 1s and F 1s peaks can be observed of pristine polyimide, whereas three main peaks of K 1s, 2p3/2, and 2p1/2 demonstrate the formation of —COOK through surface-KOH-etching treatment. After self-assembly of ZIF-8 nanocrystals, there are no notable potassium peaks. As expected, peaks of Zn 2p3/2, and 2p1/2 can be obviously observed, which suggests the ZIF-8 nanoparticles are completely cover the polyimide substrate to form continuous MOF network. In addition, the binding energy of Zn 2p3/2 in Zn^{2+} ion-exchanged polyimide is 1022.5 eV, while the binding energy of Zn 2p3/2 in self-assembled MOF network shifts to 1021.7 eV, which indicates the different coordination environments for Zn(II) species. The peak at 1022.5 eV of Zn^{2+} ion-exchanged polyimide suggests that Zn(II) species are located at the interface via coordination with carboxyl groups on the surface of polyimide substrate. And the peak at 1021.7 eV of self-assembled MOF network indicates that Zn(II) species are surrounded by four nitrogen atoms. The results conform the great feasibility of the surface etching induced self-assembly strategy to construct the hierarchically self-assembled MOF network.

Scanning electron microscopy (SEM) was performed to investigate the formation of the hierarchically self-assembled

MOF network. In this work, the pristine polyimide membrane is composed of interconnected fibers with smooth surface, forming cross-linked 3D fiber network (Figure S2a, Supporting Information). The large pores between interconnected fibers are beneficial to the full infiltration of PVDF-LiTFSI for a dense electrolyte. During self-assembly process, the spatial distribution and morphology of MOF nanoparticles can be regulated via different reaction times. At the initial stage, a thin coating of amorphous MOF nanoparticles was self-assembled on polyimide fibers (Figure S2b, Supporting Information), indicating that carboxylated polyimide could provide massive and homogeneous nucleation sites. With the prolongation of reaction time, the size of MOF nanoparticles became larger to form a denser layer (Figure S2c, Supporting Information). Further growth of the MOF nanoparticles resulted in continuous and intergrown MOF coating (Figure 2a–c), in which the well-ordered MOF nanoparticles fully cover the polyimide fibers to form 1D MOF fibers. In TEM images (Figure S4, Supporting Information), the self-assembled MOF is continuous, and the nanocrystals are extensively intergrown with neighboring ones, which plays a key role in continuous and fast ions pathways in the bulk of the composite electrolyte. The specific surface area and pore structure of the hierarchically self-assembled MOF network were analyzed by nitrogen adsorption-desorption test (Figure S6, Supporting Information). The specific surface area of the MOF network was 557.6 $m^2 g^{-1}$, which helped to accommodate more IL for high ionic conductivity, and a large number of micropores can spatially confine the movement of larger anions as ion sieves to promote Li^+ transport as well. Moreover, the successful fabrication of self-assembled MOF@IL ion conductor can be testified by XPS spectra in Figures S7 and S8 (Supporting Information) due to the emerging peaks of F1s and S 2p. In addition, the shifting binding energy of Zn 2p demonstrates the interactions between Zn sites inside ZIF-8 and $TFSI^-$ of IL, which indicates the selective bonding of $TFSI^-$, thereby promoting the fast transport of Li^+. Figure 2d depicts the photos of hierarchically self-assembled MOF network being flat, bent, squeezed and after without fracture, demonstrating its remarkable flexibility and high mechanical strength. The mechanical superiority mainly relies on the strong banding between MOF and polyimide, as well as the robustness of the polyimide skeleton. As shown in Figure 2e, PVDF-LiTFSI matrix permeates throughout the hierarchically self-assembled MOF network, and fills the interspace between interconnected fibers, the resultant composites present a relatively dense and smooth surface with the hierarchical conducting MOF network fully imbedded into the PVDF matrix.

This rational design of the hierarchically self-assembled MOF network was testified by testing ionic conductivities of different types of solid electrolytes. Pristine PVDF-LiTFSI electrolyte (PVDF) and randomly dispersed MOF@IL powder in PVDF-LiTFSI electrolyte (MOF powder-PVDF) were fabricated as contrast. **Figure 3**a shows the electrochemical impedance spectroscopy (EIS) of PVDF, MOF powder-PVDF and MOF network-PVDF solid electrolytes at 30 °C, respectively, demonstrating the lowest bulk resistance of MOF network-PVDF composite electrolytes. And the typical EIS of MOF network-PVDF composite electrolytes was examined at different temperatures from 20 to 80 °C as presented in Figure 3b. Figure 3c compares the ionic conductivities of PVDF, MOF powder-PVDF

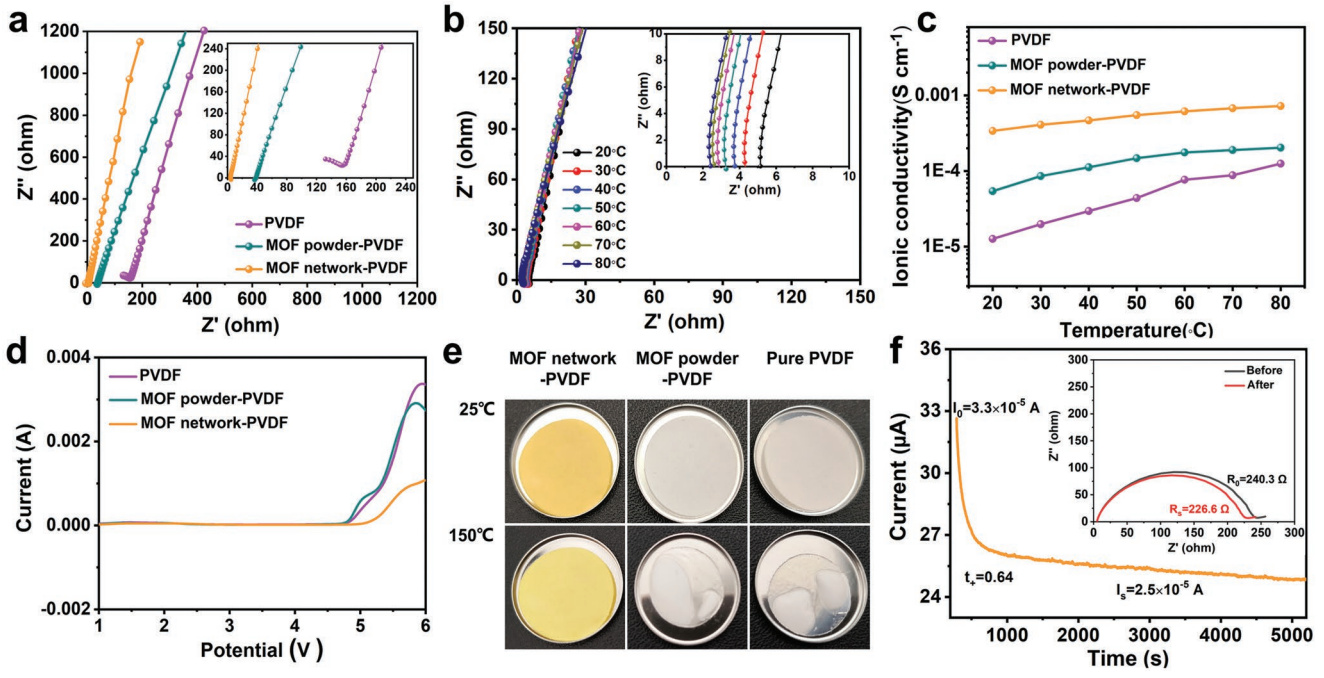

Figure 3. Ionic transport and stability of hierarchically self-assembled MOF network reinforced polymer electrolyte. a) EIS plots of different solid electrolytes at 30 °C. b) Typical EIS plots of MOF network-PVDF composite solid electrolyte at various temperatures. c) Temperature-dependent ionic conductivities of different solid electrolytes. d) linear sweep voltammetry curves of different solid electrolytes. e) In situ heating tests of different solid electrolytes. f) Current–time curves of MOF network-PVDF composite solid electrolyte in Li symmetric cell; inset: the corresponding Nyquist plots before and after polarization.

and MOF network-PVDF solid electrolytes at elevated temperatures, and Figure S12 (Supporting Information) shows the corresponding Arrhenius plots for different solid electrolytes. To be specific, ionic conductivities of PVDF are 1.98×10^{-5} S cm^{-1} at 30 °C and 7.66×10^{-5} S cm^{-5} at 60 °C, and the corresponding activation energy is 0.30 eV. With randomly dispersed MOF@IL powder as fillers, the values increase to 8.55×10^{-5} S cm^{-1} at 30 °C and 1.75×10^{-4} S cm^{-1} at 60 °C, with a decreased activation energy of 0.18 eV. Significantly, hierarchically self-assembled MOF network is superior to randomly distributed MOF powders in ionic conductivities of 4.08×10^{-4} S cm^{-1} at 30 °C and 6.17×10^{-4} S cm^{-1} at 60 °C, showing the lowest activation energy of 0.10 eV. The high ionic conductivity and low activation energy will benefit for battery performance, which reflects the lower energy barrier for Li^+ transport by the introduction of hierarchically self-assembled MOF network. Furthermore, the electrochemical-stability windows of PVDF and MOF powder-PVDF solid electrolytes are similar, both of them begin to decompose at about 4.8 V (Figure 3d). In contrast, the MOF network-PVDF composite solid electrolyte can maintain stable up to 5.2 V, reflecting its better electrochemical stability. For composite polymer electrolytes, Li^+ transference number t (Li^+) is a critical parameter to demonstrate the mobility of Li ions. A higher t (Li^+) reflects more "free Li ions" and immobilized anions, which contributes to the homogeneous transport and deposition of Li ions and thus avoids the lithium dendrite formation and growth. Figure 3f shows the polarization curve as well as initial and steady state impedance diagram of symmetric Li cell with MOF network-PVDF solid electrolyte. The polarization current began to decline from 3.3×10^{-5} A and maintained stable at 2.5×10^{-5} A. The initial impedance (R_0) was simulated to be 240.3 Ω and decreased to 226.6 Ω of the steady impedance (R_s). Based on this, the t (Li^+) was calculated to be 0.64, which can be ascribed to the fact that the hierarchically self-assembled MOF network can provide continuous linear pathways for Li^+. Besides, sub-nano pores in MOF nanocrystals can spatially confine the movement of larger anions as ion sieves to promote Li^+ transport, and the open metal sites showing Lewis acid feature enable the selective bonding of $TFSI^-$, thus liberating more free Li^+. The high t (Li^+) can contribute to uniform deposition of Li^+ and thereby effectively inhibit the growth of lithium dendrites and highly improve the safety of batteries.

In addition to above electrochemical properties, thermal stability and mechanical robustness are also significant criterions for composite solid electrolytes. In situ heating tests of the three kinds of solid electrolytes in this work (Figure 3e), MOF network-PVDF composite solid electrolyte could remain stable structure after being heated at 150 °C for 30 min because of the remarkable thermal stability of the hierarchically self-assembled MOF network. In sharp contrast, both of PVDF and MOF powder-PVDF solid electrolytes suffered from huge structural failure as a result of the softening PVDF matrix at high temperature and lack of support skeleton with desired thermal stability, which is prone to lithium dendrite penetration. Moreover, thermal-gravimetric (TG) results (Figure S10, Supporting Information) illustrate that the MOF network-PVDF composite solid electrolyte can be thermally stable to about 370 °C, demonstrating the great thermal stability. Before 370 °C, the early mass loss of 9.12% is related to absorbed moisture from air and trapped DMF solvent in PVDF. Based on this, hierarchically self-assembled MOF network can effectively eliminate the thermal-runaway risks and simultaneously promote safety at high temperature because of its excellent thermal stability.

As can be seen in **Figure 4**c, the tensile strength of pure PVDF solid electrolyte is 4.98 MPa, and increases to 6.41 MPa with randomly distributed MOF powder as fillers. However, this limited enhancement of mechanical strength derived from traditional powder is far from practical demands. To further improve the robustness of PVDF-based polymer electrolytes, the embedment of hierarchically self-assembled MOF network could yield a highly improved tensile strength of 22.02 MPa. The high mechanical strength can be attributed to intrinsic advantage in mechanical property of the hierarchically self-assembled MOF network. In addition, MOF nanocrystals are strongly attached to the polyimide substrate, which plays a key role in the excellent structure stability of the hierarchically self-assembled MOF network, thus enabling the continuous Li^+ conduction and inhibiting the growth of lithium dendrites for higher safety. The robustness of the self-assembled MOF network was tested via vigorous stirring (600 rpm) of the self-assembled MOF network in methanol for 48 h. As a result, no obvious loss of MOF nanocrystals can be observed by SEM images (Figure S13, Supporting Information), which confirms the strong banding between MOF and polyimide. Theoretically, high ionic conductivity and mechanical strength can reinforce the dendrite-suppressing capability of composite solid electrolytes, which was demonstrated by long-term Li plating/stripping tests with Li–Li symmetrical cells. At the current density of 0.1 mA cm^{-2} (Figure 4a), the batteries with pure PVDF solid electrolyte delivered increased polarization voltage within 170 h and suddenly short-circuited at 170 h. With the assistance of randomly distributed MOF@IL powder as fillers, the Li-Li cells could be stable within 1500 h. When the randomly distributed MOF powder was self-assembled to the hierarchically self-assembled MOF network, the cells could work stably with the lowest polarization voltage more than 1500 h. More importantly, when cycled at higher current density of 0.4 mA cm^{-2} (Figure 4b), MOF network-PVDF composite solid electrolyte also displayed a highly stable cycling performance thanks to the favorable hierarchically self-assembled structure (Figure 4g). In contrast, MOF powder-PVDF and pure PVDF solid electrolytes show noticeably unstable and short-circuited cyclic performance, respectively, indicating the poor ability to suppress the growth of lithium dendrites and uneven deposition of Li ions (Figure 4e,f).[42,43] To further confirm the dendrite-suppressing capability of the three solid electrolytes, lithium anodes after 1100 h cycle at 0.4 mA cm^{-2} was directly investigated by SEM images. Figure S15a,b (Supporting Information) shows numerous loose and porous "dead Li" on the surface of lithium anodes assembled with pure PVDF and MOF powder-PVDF solid electrolytes, respectively, which were in good consistent with the results of Li plating/stripping in symmetric Li–Li batteries. By contrast, lithium anode associated with MOF network-PVDF composite solid electrolyte presented smooth and dense surface without obvious lithium dendrites (Figure S15c, Supporting Information), suggesting the efficient resistance of Li dendrite growth by the introduction of the hierarchically self-assembled MOF network.

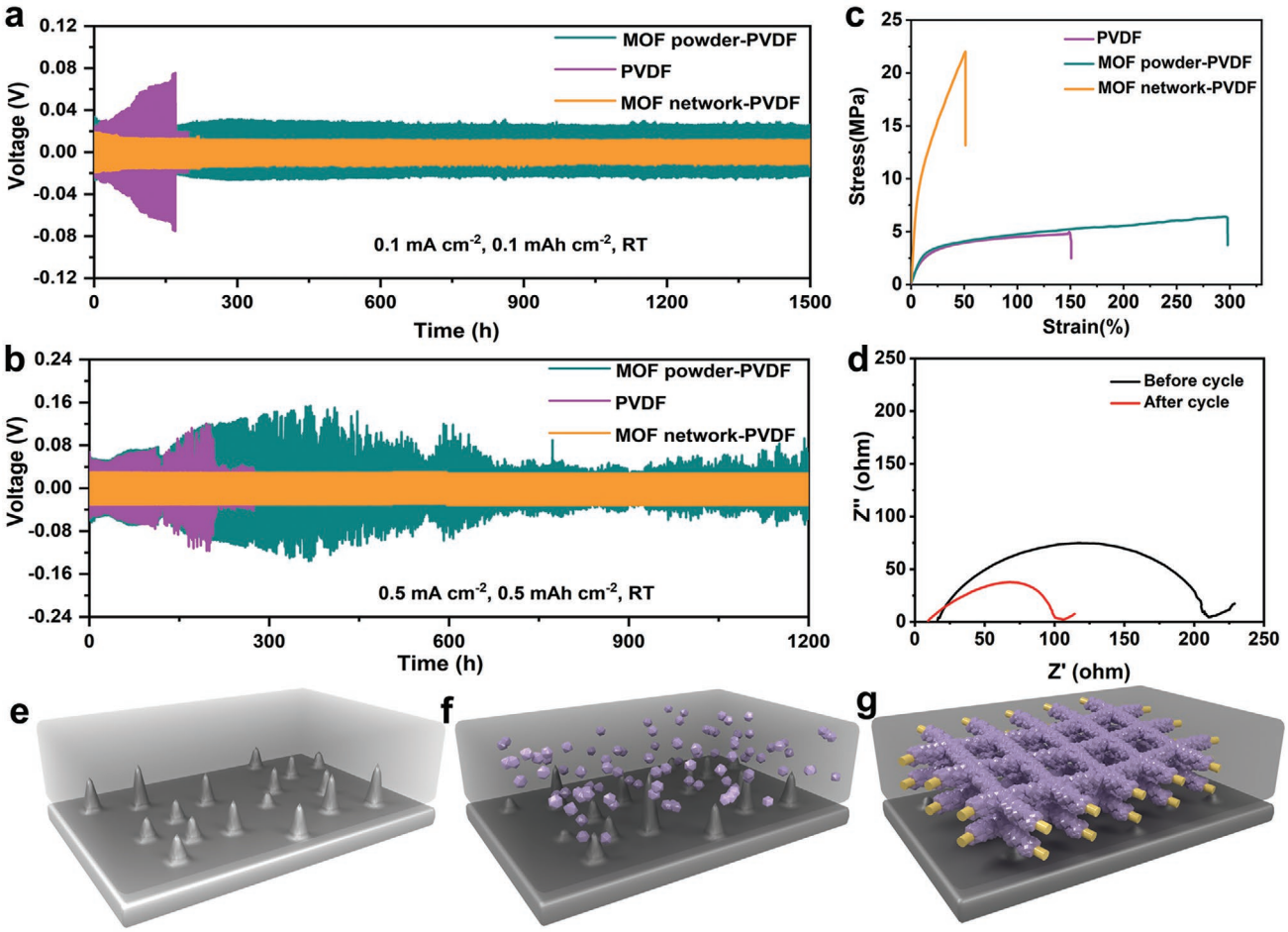

Figure 4. Li symmetric cells with hierarchically self-assembled MOF network reinforced polymer electrolyte. a,b) Cycling performance of Li symmetric cells with different solid electrolytes at current densities of 0.1 and 0.4 mA cm^{-2} at room temperature, respectively. c) Stress–strain curves of different solid electrolytes. d) Electrochemical impedance of Li symmetric cell with MOF network-PVDF before and after cycle. Schematic illustrations of Li dendrite behaviors in different solid electrolytes: e) PVDF, f) MOF powder-PVDF, and g) MOF network-PVDF.

Eventually, $LiFePO_4$//Li solid-state batteries with different solid electrolytes were fabricated to investigate their potential for wide applications. **Figure 5**a compares the rate performances of batteries with different solid electrolytes at room temperature. The batteries fabricated with MOF network-PVDF composite solid electrolytes delivered average discharge capacities of 161.4, 155.0, 147.0, 135.2, and 126.0 mAh g^{-1} at current rates of 0.2, 0.5, 1, 2, and 3 C, respectively, and simultaneously present great capacity reversibility when the rate returning back to lower rate of 0.2 C, which indicated the remarkable electrochemical stability under large current density. This excellent rate performance could be attributed to rational design of the hierarchically self-assembled MOF network, which can provide continuous and long-range Li^+ transfer channels, thus contributing to the fast Li^+ transfer within the full cell system. In contrast, the cells using pure PVDF and MOF powder-PVDF solid electrolytes displayed lower average discharge capacities at the same rates than those of cells using self-assembled MOF network. Particularly, the severely decreased discharge capacities such as 63.5 and 88.0 mAh g^{-1} at 3 C reveal the insufficient Li^+ transport in pure PVDF and MOF powder-PVDF solid electrolytes. Meanwhile, Figure 5b illustrates charge-discharge curves of batteries with MOF network-PVDF composite solid electrolytes at current rates of 0.2, 0.5, 1, 2, and 3 C, and the discharge voltage plateau slightly decline with negligible polarization along with the increased rates.

Another important criterion to evaluate applicability of composite solid electrolytes is long-time cyclic stability in full batteries. Figure 5c shows the room-temperature cycling performances at 0.5 C of full batteries using different solid electrolytes prepared in this work. The cells using pure PVDF solid electrolyte show exceedingly poor cyclic stability with a capacity retention of 31% after 200 cycles. When adding traditional MOF powder as fillers into the PVDF matrix, the cycling performance was improved, resulting a capacity retention of 77.8% after 200 cycles, but it is impracticable for long-life batteries. Prominently, self-assembly of randomly distributed MOF powder onto polyimide fibers to form hierarchically self-assembled MOF network resulted in an enhanced discharge capacity, higher coulombic efficiency and desired cycling stability. To be specific, the MOF network-PVDF-based full batteries can maintain a rather high capacity retention of 96.0%

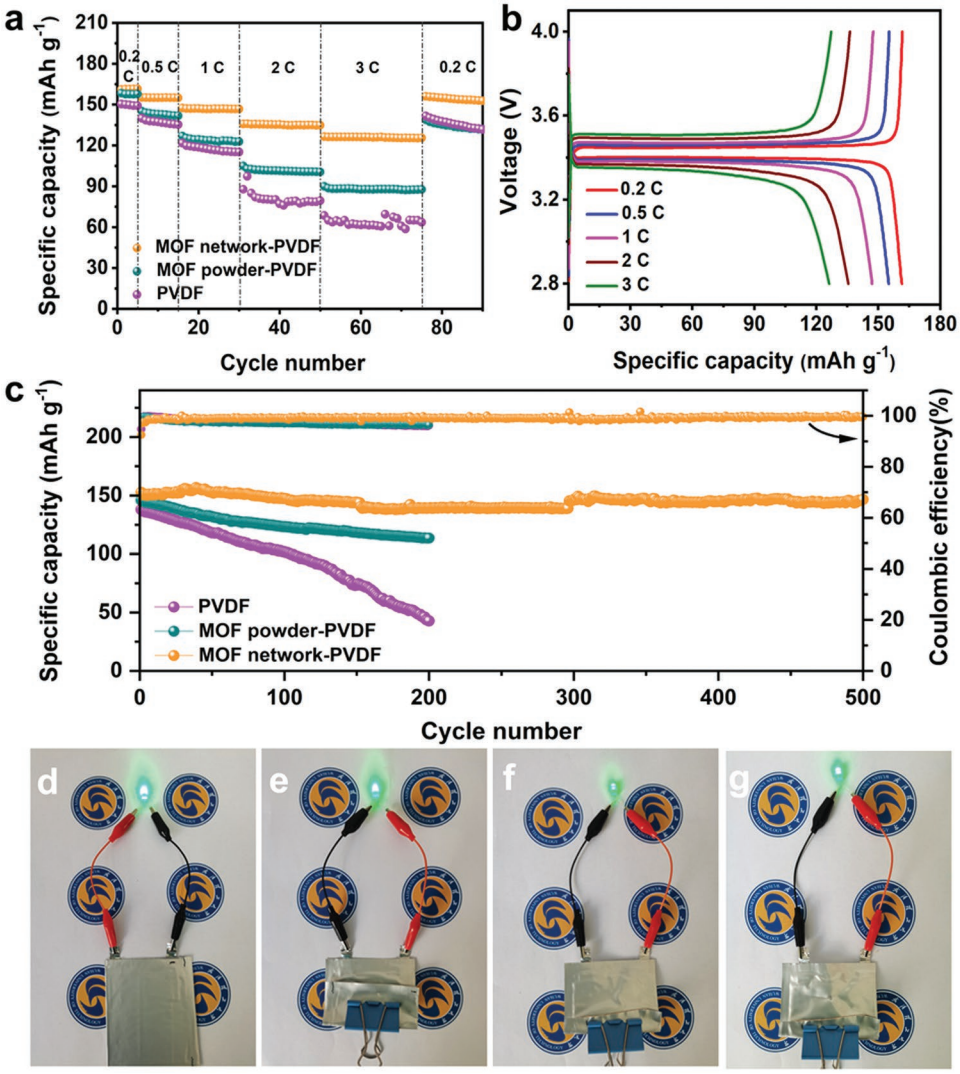

Figure 5. Electrochemical properties of solid-state $LiFePO_4$//Li batteries with hierarchically self-assembled MOF network reinforced polymer electrolyte. a) Rate performances with different solid electrolytes. b) Charge and discharge voltage profiles at different rates with MOF network-PVDF composite solid electrolyte. c) Cycling performances with different solid electrolytes. Photos of solid-state pouch Li metal cell based on MOF network-PVDF composite solid electrolyte showing well-running at d) Flat, e) Bending, f) Cutting, and g) Punching states.

after 500 cycles at 0.5 C rate, meaning a decay rate of 0.008% per cycle, which merely decreased from 152.6 to 146.6 mAh g^{-1}. And its Coulombic efficiency can reach up to 99.61% after 500 cycles, which is in accord with the desirable cyclic performance. Besides, the MOF network-PVDF composite solid electrolyte also shows remarkable battery performance coupled with high-voltage $LiNi_{0.8}Co_{0.1}Mn_{0.1}O_2$ (NCM811) as cathode between 2.6 and 4.3 V, which indicates the great electrochemical stability of the MOF network-PVDF composite solid electrolyte (Figure S17, Supporting Information). In addition to these, safety really matters for practical use of batteries. The $LiFePO_4$/MOF network-PVDF/Li pouch cell was fabricated to demonstrate the high-safety merit of the hierarchically self-assembled MOF network under destructive conditions. As shown in Figure 5d–g, the pouch cell worked well even under conditions of being folded, cut and nail penetrated, reflecting reliable and safe property of the hierarchically self-assembled MOF network. All above results demonstrate the great potential of the ingenious design of hierarchically self-assembled MOF network in state-of-the-art composite solid electrolytes.

3. Conclusion

In conclusion, a hierarchically self-assembled MOF network for composite solid electrolytes was developed, and the resultant composite is characteristic of high ionic conductivity of 4.08×10^{-4} S cm^{-1} at 30 °C and high mechanical strength of 22.0 MPa. This monolithic 3D ion conductor consists of interconnected 1D MOF fibers, forming a unique hierarchical ion-conducting network. At the micrometer scale, each 1D MOF fiber can provide continuous pathways for Li^+ along the 1D direction. Moreover, sub-nano pores and the open metal sites in MOF nanocrystals can selectively confine the movement of larger anions as ion sieves to promote Li^+ transport.

In addition, the strong banding between MOF and polyimide, coupled with the robustness of the polyimide skeleton, endows the MOF network with high mechanical strength and flexibility. Because of above merits, the assembled Li–Li cells perform well without short circuit and the corresponding solid-state $LiFePO_4$//Li cells maintain a remarkable capacity retention of 96.0% after 500 cycles at 0.5 C rate, from 152.6 to 146.6 mAh g^{-1} at room temperature. This work shows the great prospect for spatial arrangement of incorporated powders by self-assembled strategy in composite solid electrolytes toward both high ionic conductivity and mechanical strength.

Supporting Information

Supporting Information is available from the Wiley Online Library or from the author.

Acknowledgements

This work was supported by the National Key Research and Development Program of China (2020YFA0715000), the Key Research and Development Program of Hubei Province (2021BAA070), the National Natural Science Foundation of China (51802239 and 51832004), Foshan Xianhu Laboratory of the Advanced Energy Science and Technology Guangdong Laboratory (XHT2020-005 and XHT2020-003), the Natural Science Foundation of Hubei Province (2019CFA001), the Youth Innovation Research Fund Project of State Key Laboratory of Advanced Technology for Materials Synthesis and Processing at Wuhan University of Technology, and the Fundamental Research Funds for the Central Universities (2020III011GX, 2020IVB057, 2019IVB054, and 2019III062JL).

Conflict of Interest

The authors declare no conflict of interest.

Data Availability Statement

The data that support the findings of this study are available from the corresponding author upon reasonable request.

Keywords

composite solid electrolytes, continuous ion transport, flexibility, mechanical strength, self-assembled MOF networks

Received: February 10, 2022
Revised: April 7, 2022
Published online:

[1] C. Avci, I. Imaz, A. Carne-Sanchez, J. A. Pariente, N. Tasios, J. Perez-Carvajal, M. I. Alonso, A. Blanco, M. Dijkstra, C. Lopez, D. Maspoch, *Nat. Chem.* **2018**, *10*, 78.
[2] W. Fu, J. S. Qiao, X. X. Zhao, Y. Chen, D. Y. Fu, W. Yu, K. Leng, P. Song, Z. Chen, T. Yu, S. J. Pennycook, S. Y. Quek, K. P. Loh, *ACS Nano* **2020**, *14*, 3917.
[3] K. X. Chen, L. Li, *Adv. Mater.* **2019**, *31*, 7.
[4] B. Munkhbat, A. Canales, B. Kucukoz, D. G. Baranov, T. O. Shegai, *Nature* **2021**, *597*, 214.
[5] G. M. Whitesides, B. Grzybowski, *Science* **2002**, *295*, 2418.
[6] L. B. Mao, H. L. Gao, H. B. Yao, L. Liu, H. Colfen, G. Liu, S. M. Chen, S. K. Li, Y. X. Yan, Y. Y. Liu, S. H. Yu, *Science* **2016**, *354*, 107.
[7] Z. G. Zhao, R. C. Fang, Q. F. Rong, M. J. Liu, *Adv. Mater.* **2017**, *29*, 16.
[8] C. T. Zuo, A. Scully, D. Yak, W. L. Tan, X. C. Jiao, C. R. McNeill, D. C. Angmo, L. M. Ding, M. Gao, *Adv. Energy Mater.* **2019**, *9*, 1803258.
[9] M. L. Aubrey, A. S. Valdes, M. R. Filip, B. A. Connor, K. P. Lindquist, J. B. Neaton, H. I. Karunadasa, *Nature* **2021**, *597*, 355.
[10] R. W. Yi, Y. Y. Mao, Y. B. Shen, L. W. Chen, *J. Am. Chem. Soc.* **2021**, *143*, 12897.
[11] L. Z. Fan, H. C. He, C. W. Nan, *Nat. Rev. Mater.* **2021**, 17.
[12] Y. Cheng, J. Shu, L. Xu, Y. Y. Xia, L. L. Du, G. Zhang, L. Q. Mai, *Adv. Energy Mater.* **2021**, *11*, 9.
[13] S. Tang, W. Guo, Y. Z. Fu, *Adv. Energy Mater.* **2021**, *11*, 29.
[14] S. Stramare, V. Thangadurai, W. Weppner, *Chem. Mater.* **2003**, *15*, 3974.
[15] L. Q. Xu, J. Y. Li, W. T. Deng, H. L. Shuai, S. Li, Z. F. Xu, J. H. Li, H. S. Hou, H. J. Peng, G. Q. Zou, X. B. Ji, *Adv. Energy Mater.* **2021**, *11*, 24.
[16] Z. L. Jian, Y. S. Hu, X. L. Ji, W. Chen, *Adv. Mater.* **2017**, *29*, 1601925.
[17] Y. Yoshida, K. Fujie, D. W. Lim, R. Ikeda, H. Kitagawa, *Angew. Chem., Int. Ed.* **2019**, *58*, 10909.
[18] D. X. Li, J. Wang, S. J. Guo, Y. B. Xiao, Q. H. Zeng, W. C. He, L. Y. Gan, Q. Zhang, S. M. Huang, *Adv. Funct. Mater.* **2020**, *30*, 8.
[19] Q. Zhang, B. M. Liu, J. Wang, Q. F. Li, D. X. Li, S. J. Guo, Y. B. Xiao, Q. H. Zeng, W. C. He, M. Y. Zheng, Y. F. Ma, S. M. Huang, *ACS Energy Lett.* **2020**, *5*, 2919.
[20] Q. H. Zeng, J. Wang, X. Li, Y. Ouyang, W. C. He, D. X. Li, S. J. Guo, Y. B. Xiao, H. Y. Deng, W. Gong, Q. Zhang, S. M. Huang, *ACS Energy Lett.* **2021**, *6*, 2434.
[21] M. Yao, T. H. Yu, Q. Q. Ruan, Q. J. Chen, H. T. Zhang, S. J. Zhang, *ACS Appl. Mater. Interfaces* **2021**, *13*, 47163.
[22] H. C. Wang, Q. Wang, X. Cao, Y. Y. He, K. Wu, J. J. Yang, H. H. Zhou, W. Liu, X. M. Sun, *Adv. Mater.* **2020**, *32*, 9.
[23] W. Y. Shi, J. Q. Shen, L. Shen, W. Hu, P. C. Xu, J. A. Baucom, S. X. Ma, S. X. Yang, X. M. Chen, Y. F. Lu, *Nano Lett.* **2020**, *20*, 5435.
[24] W. Liu, N. Liu, J. Sun, P. C. Hsu, Y. Z. Li, H. W. Lee, Y. Cui, *Nano Lett.* **2015**, *15*, 2740.
[25] B. Y. Li, Q. M. Su, L. T. Yu, D. Wang, S. K. Ding, M. Zhang, G. H. Du, B. S. Xu, *ACS Appl. Mater. Interfaces* **2019**, *11*, 42206.
[26] S. Hu, L. L. Du, G. Zhang, W. Y. Zou, Z. Zhu, L. Xu, L. Q. Mai, *ACS Appl. Mater. Interfaces* **2021**, *13*, 13183.
[27] M. M. Zhang, P. Pan, Z. L. Cheng, J. T. Mao, L. Y. Jiang, C. K. Ni, S. K. Park, K. Y. Deng, Y. Hu, K. K. Fu, *Nano Lett.* **2021**, *21*, 7070.
[28] C. Wang, D. F. Huang, S. H. Li, J. M. Yu, M. W. Zhu, N. Liu, Z. D. Lu, *Nano Lett.* **2020**, *20*, 7397.
[29] A. C. Balazs, T. Emrick, T. P. Russell, *Science* **2006**, *314*, 1107.
[30] K. Fu, Y. H. Gong, J. Q. Dai, A. Gong, X. G. Han, Y. G. Yao, C. W. Wang, Y. B. Wang, Y. N. Chen, C. Y. Yan, Y. J. Li, E. D. Wachsman, L. B. Hu, *Proc. Natl. Acad. Sci. USA* **2016**, *113*, 7094.
[31] J. Bae, Y. T. Li, J. Zhang, X. Y. Zhou, F. Zhao, Y. Shi, J. B. Goodenough, G. H. Yu, *Angew. Chem., Int. Ed.* **2018**, *57*, 2096.
[32] H. W. Zhai, P. Y. Xu, M. Q. Ning, Q. Cheng, J. Mandal, Y. Yang, *Nano Lett.* **2017**, *17*, 3182.
[33] J. Bae, Y. T. Li, F. Zhao, X. Y. Zhou, Y. Ding, G. H. Yu, *Energy Storage Mater.* **2018**, *15*, 46.
[34] X. Wang, H. W. Zhai, B. Y. Qie, Q. Cheng, A. J. Li, J. Borovilas, B. Q. Xu, C. M. Shi, T. W. Jin, X. B. Liao, Y. B. Li, X. D. He, S. Y. Du, Y. K. Fu, M. Dontigny, K. Zaghib, Y. Yang, *Nano Energy* **2019**, *60*, 205.

[35] J. M. Yu, T. L. Guo, C. Wang, Z. H. Shen, X. Y. Dong, S. H. Li, H. G. Zhang, Z. D. Lu, *Nano Lett.* **2021**, *21*, 5805.
[36] J. Y. Wan, J. Xie, X. Kong, Z. Liu, K. Liu, F. F. Shi, A. Pei, H. Chen, W. Chen, J. Chen, X. K. Zhang, L. Q. Zong, J. Y. Wang, L. Q. Chen, J. Qin, Y. Cui, *Nat. Nanotechnol.* **2019**, *14*, 705.
[37] J. K. Hu, P. G. He, B. C. Zhang, B. Y. Wang, L. Z. Fan, *Energy Storage Mater.* **2020**, *26*, 283.
[38] D. Ai, H. Li, Y. Zhou, L. L. Ren, Z. B. Han, B. Yao, W. Zhou, L. Zhao, J. M. Xu, Q. Wang, *Adv. Energy Mater.* **2020**, *10*, 1903881.
[39] K. Akamatsu, S. Ikeda, H. Nawafune, S. Deki, *Chem. Mater.* **2003**, *15*, 2488.
[40] S. X. Mu, Z. P. Wu, Y. Wang, S. L. Qi, X. P. Yang, D. Z. Wu, *Thin Solid Films* **2010**, *518*, 4175.
[41] S. Ikeda, K. Akamatsu, H. Nawafune, T. Nishino, S. Deki, *J. Phys. Chem. B* **2004**, *108*, 15599.
[42] X. Meng, K. C. Lau, H. Zhou, S. K. Ghosh, M. Benamara, M. Zou, *Energy Mater. Adv.* **2021**, *2021*, 9786201.
[43] H. Gao, N. S. Grundish, Y. Zhao, A. Zhou, J. B. Goodenough, *Energy Mater. Adv.* **2021**, *2021*, 1932952.